Available on CMS information server

CMS AN -2010/212

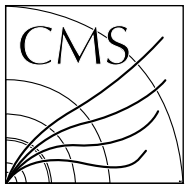

The Compact Muon Solenoid Experiment

Analysis Note

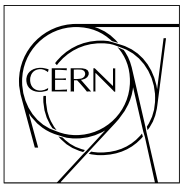

30 June 2010

An algorithm for the determination of the flight path of long-lived particles decaying into photons

D. Franci, S. Rahatlou, D. del Re

Abstract

A model-independent approach to identify long-lived particles decaying into photons is presented. A combined selection based on both the ECAL time and cluster shape moments is used to select off-pointing photons. Moreover, reconstructed momentum of the off-pointing photon used in combination with the ECAL time allows a precise measurement of the flight path of the long- lived particle.

Contents

1 Introduction

Many physics scenarios beyond the Standard Model (SM) predict the existence of massive, neutrally charged, long-lived particles decaying into photons. Since these particles are predicted to have relatively long lifetimes, the decaying photons will not originate from interaction point and are hence referred to as 'off-pointing'. Subsequently, these off-pointing photons provide a clear signature for decays of this type, and also give an indication of new physics scenarios. We use information from the CMS electromagnetic calorimeter (ECAL), namely the reconstructed photon time measurement and the shape of the energy deposit in order to select off-pointing photons. We also demonstrate that the ECAL provides an excellent resolution for the time measurement, and offers a fine lateral granularity allowing for complex studies on the geometry of ECAL cluster deposits, which are exploited. We then present an algorithm to extract the flight path for long-lived particles decaying into photons.

Although we follow a model-independent approach, our study will focus on the Gauge Mediated Supersymmetry Breaking (GMSB) model [1]. The GMSB model accounts for the neutralino (χ_1^0) as the Next to Lightest Supersymmetric Particle (NLSP) decaying into a gravitino plus photon ($\chi_1^0 \rightarrow \tilde{G}\gamma$). According to the choice of model parameters, the neutralino lifetime can be non-zero which would produce a sample of off-pointing photons. We also present selection criteria for off-pointing photons based on both the ECAL time measurement, and the spread of the ECAL energy deposit. Once a clean sample of off-pointing photons has been attained, we extract the momenta of the photons using the energy measurement, and a set of variables which describe the geometrical properties for the shape of the energy deposits in the ECAL. These variables are commonly referred to as *cluster shape variables*. Lastly, we use the photon momentum in combination with the ECAL time measurement in order to extract the neutralino flight path. This note is organised as follows:

- Section 2 - Description of the datasets used;
- Section 3 - Description of the selection criteria for off-pointing photons;
- Section 4 - Description of the algorithm use to reconstruct the flight path of the long-lived particle;
- Section 5 - Summary and conclusion.

2 Datasets

The GMSB datasets used for this study follows line 8 of the Snowmass points and slopes (SPS 8) proposal [2], where the parameters used are reported in Table 1.

GMSB SPS 8 line				
M_m	N	$tan\beta$	$sign(\mu)$	Λ
$2 \cdot \Lambda$	1	15	+1	free

Table 1: GMSB SPS 8 line.

This choice ensures that the χ_1^0 in the $\chi_1^0 \rightarrow \tilde{G}\gamma$ decay is the NLSP with a branching ratio close to 100%. The SUSY breaking scaling parameter, Λ (which is left free in the SPS 8 line), is set to $\Lambda = 100$ TeV. This choice sets the neutralino mass ($M_{\chi_1^0}$) to be 135.3 GeV.

In order to investigate the detection capabilities of the ECAL for long-lived particles of this type, we create signal datasets using four different values of the χ_1^0 lifetime. This is done by varying the value of the C_{grav} parameter to:

- $C_{grav} = 46.7$ for $c\tau = 250$ mm;
- $C_{grav} = 66.1$ for $c\tau = 500$ mm;
- $C_{grav} = 93.5$ for $c\tau = 1000$ mm;
- $C_{grav} = 132.2$ for $c\tau = 2000$ mm;

Signal datasets are the generated and reconstructed using CMSSW_3_5_6, using the full CMS detector simulation at center of mass energy $\sqrt{s} = 7$ TeV.

3 Off-pointing photon selection

The photon from the decay of the long-lived particle has a very distinctive signature, and the excellent precision in time measurement obtained from the ECAL makes it possible to identify photons which reach the calorimeter after particles which travel at the speed of light from the interaction point. Moreover, we can recognise an off-pointing photon from the characteristic shape of its energy deposit in the ECAL.

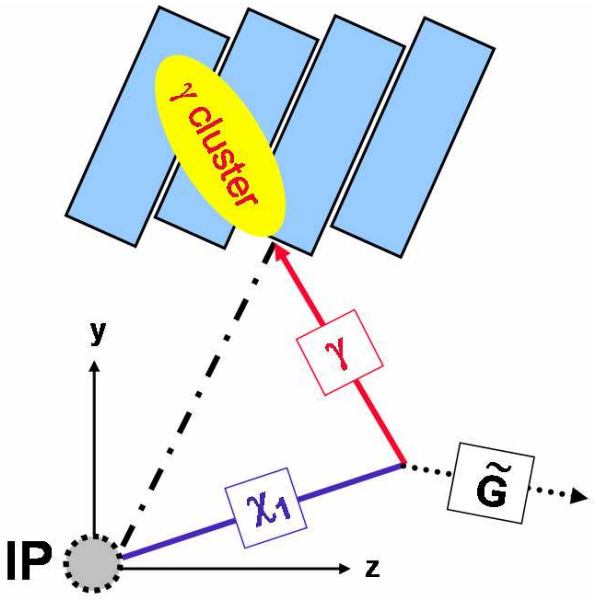

Figure 1: A schematic diagram of the long-lived $\chi_1^0 \to \tilde{G}\gamma$ neutralino decay.

Figure 1 shows a schematic view of of the $\chi_1^0 \to \tilde{G}\gamma$ neutralino decay, where the blue line represents the neutralino path length, and the red arrow indicates the direction of travel for the off-pointing photon. The graviton (which is stable, neutral, and weak-interacting) usually escapes from detection.

3.1 ECAL timing

A combination of the scintillation timescale for the $PbWO_4$ crystals in the ECAL, the electronic pulse shaping, and the sampling rate allow for an excellent time resolution to be obtained. After a signal has been amplified and shaped by the front-end electronics, the ECAL time reconstruction can be defined by a measurement of T_{max}. We define T_{max} as the time the pulse reaches its maximum value, A_{max}. We can see in Figure 2 an example of the time sampling for a signal pulse as a function of the time difference, $T - T_{max}$, where T indicates the time of the generic ADC sample.

The algorithm used to extract T_{max} is described in detail in [3], where the time resolution is shown to be less than 100 ps for energy deposits larger than 10-20 GeV in the barrel. Assuming a decay path length of 10 cm for the long-lived particle, the ECAL time measurement would equate to around 350 ps, which is considerably larger than the typical time measurement for a in-time photon. We see in Figure 3 the time distribution for the most energetic ECAL crystal on a sample of Particle Gun pointing photons, generated with energy $10 < E < 100$ GeV, within the barrel region ($|\eta| < 1.479$).

The time resolution (about 270 ps) is worse than expected, due to the fact that the detector simulation was performed using startup conditions for the ECAL. Figure 4 shows a comparison between the time distributions of the most energetic ECAL crystal for photons from the Particle Gun generator (in blue), and from GMSB neutralino decay (in red), where the χ_1^0 lifetime is set to $c\tau = 500$ mm, demonstrating the ECAL time as a powerful variable in identifying off-pointing photons.

Note that almost all the in-time photons are rejected by requiring $T_{REC} > 0.8$ ns, validating the capability of ECAL time measurement to select off-pointing photons. The ECAL time measurement can also be used to extract the total time of flight T_{TRUE}, defined as:

$$T_{TRUE} = T_{\chi_1^0} + T_\gamma \tag{1}$$

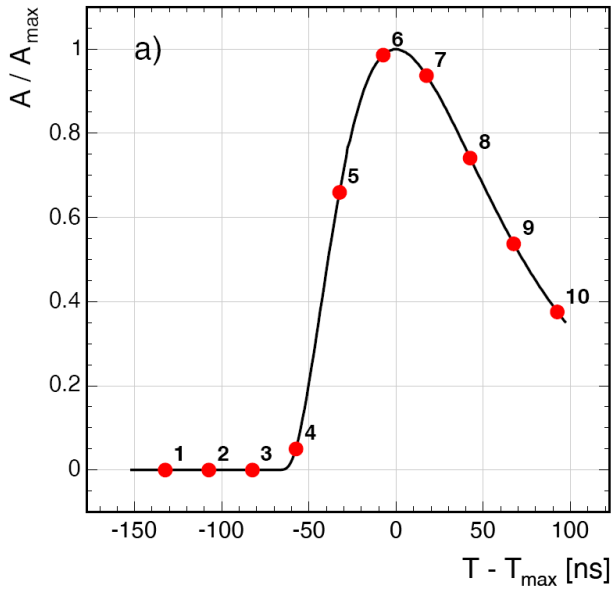

Figure 2: Pulse shape measured in ECAL as a function of $T - T_{max}$.

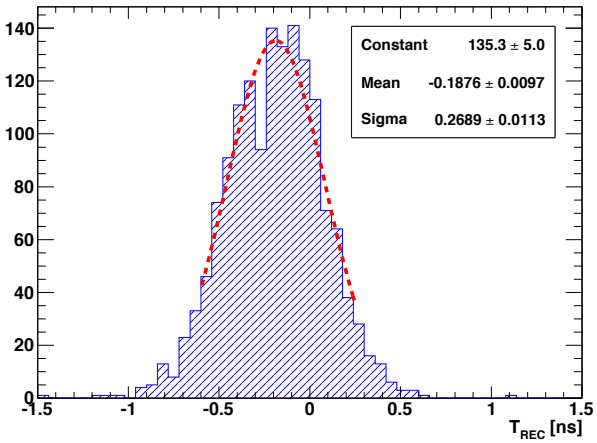

Figure 3: Time measurement distribution for a sample of Particle Gun photons. We superimpose a gaussian fit of the peak distribution.

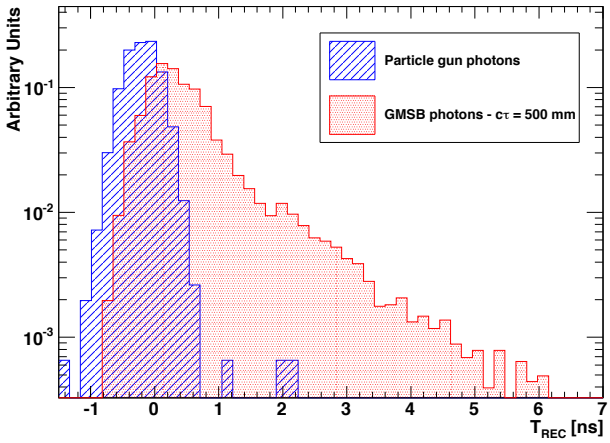

Figure 4: The ECAL time distributions for photons from the Particle Gun generator (in blue), and from the GMSB neutralino decay (with $c\tau = 500$ mm).

where $T_{\chi_1^0}$ is the neutralino decay time, and T_γ is the time at which the photon from the neutralino decay reaches the ECAL. A scatter plot of T_{REC} versus T_{TRUE} is shown in Figure 5. The histogram profile has been fitted with a linear function obtaining the following parametrization for T_{TRUE}:

$$T_{TRUE} = 0.145 + 1.03 \cdot T_{REC} \quad [ns] \tag{2}$$

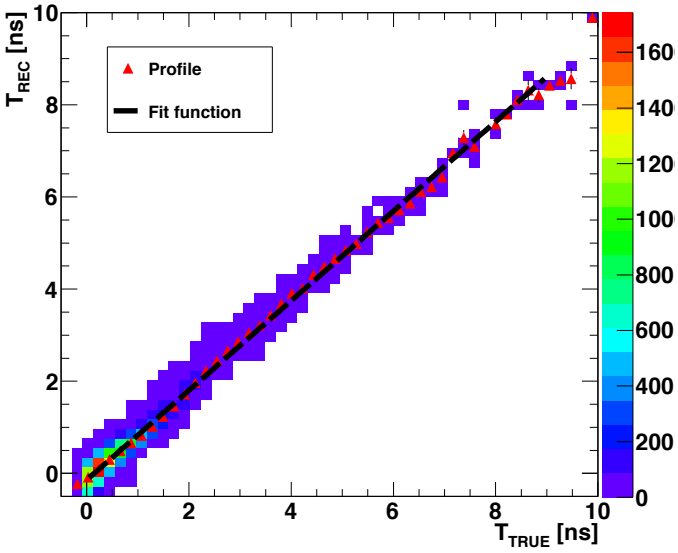

Figure 5: A scatter plot of T_{REC} versus T_{TRUE}.

Figure 6 shows the uncertainty in the determination of the total time of flight using Equation 2. We see that the ECAL time measurement provides a very precise determination for the total time of flight, where the uncertainty stays at a constant value of around 200 ps as a function of T_{TRUE}.

3.2 Principal axes of the ECAL cluster

Another distinctive feature of an off-pointing photon is the shape of the energy deposit in the ECAL. Due to the quasi-projective geometry of the calorimeter, the direction of a photon which does not point to the CMS interaction point will form a non-zero angle, δ, with the axis of the ECAL crystal, which is demonstrated in Figure 7. As a consequence, the energy deposit of an off-pointing photon produces an elliptical shape.

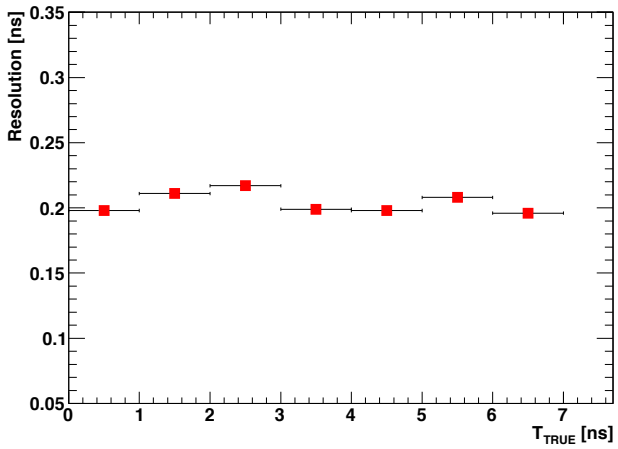

Figure 6: The uncertainty in the determination of the total time of flight as a function of T_{TRUE}.

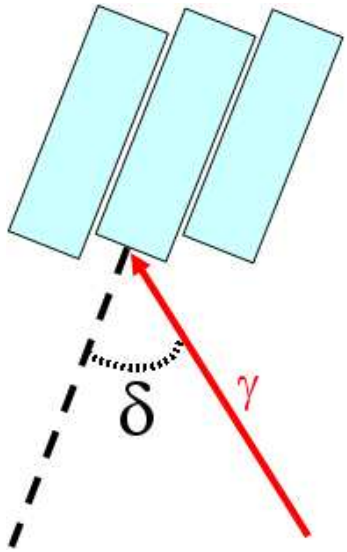

Figure 7: The angle of incidence, δ, between the axis of the ECAL crystal and the direction of the off-pointing photon.

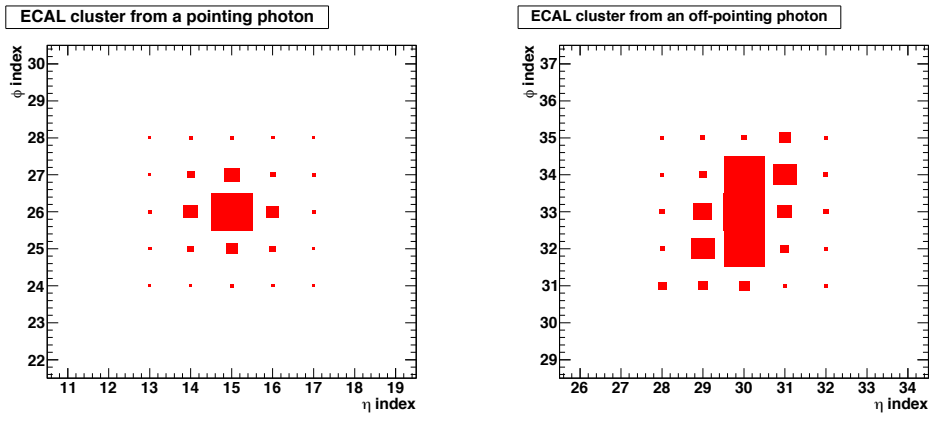

(a) (b)

Figure 8: Energy deposits in the ECAL: a) from a pointing photon; b) and from an off-pointing photon.

Figure 8 shows an example of the cluster shape for pointing, and off-pointing photons where the geometrical properties of an energy deposit in the ECAL can be described by the following covariance matrix:

$$COV_{\eta\phi} = \begin{pmatrix} \sigma_{\eta\eta} & \sigma_{\eta\phi} \\ \sigma_{\phi\eta} & \sigma_{\phi\phi} \end{pmatrix} \tag{3}$$

with,

$$S_{\mu\nu} = \sum_{i=1}^{N} w_i \left(\mu_i - \langle\mu\rangle\right)\left(\nu_i - \langle\nu\rangle\right) \tag{4}$$

where N is number of crystals in the cluster, μ_i and ν_i are the η and ϕ indexes that identify the i-th crystal of the cluster, and $\langle\mu\rangle = \frac{\sum_i w_i \cdot \mu_i}{\sum_i w_i}$. The logarithmic weight w_i defined as:

$$w_i = \max\left[K + log\left(\frac{E_i}{E_{CLUSTER}}\right); 0\right] \tag{5}$$

is used to calculate the cluster position [4]. The covariance matrix can be diagonalised in order to find the major and minor axes of the ellipse from the energy deposit. So

$$COV_{\eta\phi} = \begin{pmatrix} S_{major} & 0 \\ 0 & S_{minor} \end{pmatrix} \tag{6}$$

Here the major axis represents the projection of the photon direction on the ECAL cylinder, where the eigenvalue S_{major} is the standard deviation of the energy distribution calculated along the major axis. This variable has been previously used to discriminate energy deposits from photons and neutral pions [5].

The S_{major} distribution for pointing and off-pointing photons are shown in Figure 9. As expected we see large S_{major} for off-pointing photons with respect to clusters from pointing photons [1)]

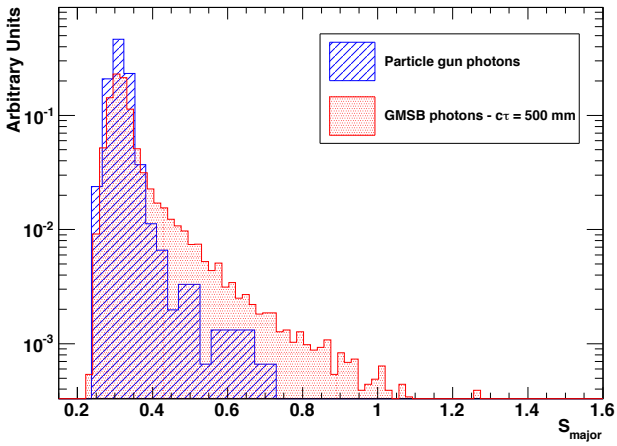

Figure 9: The S_{major} distribution for photons from the Particle Gun generator (in blue), and from the GMSB neutralino decay (with $c\tau = 500$ mm). Only unconverted photons are considered.

We also use S_{major} to obtain an estimate for the angle of incidence, δ, for an off-pointing photon with respect to the ECAL surface, where the correlation between S_{major} and $\sin\delta$ is shown in Figure 10. The profile of the scatter plot (red points in the plot) is fitted using a parabolic function, where we obtain the following parametrisation for $\sin(\delta)$:

[1)] The distributions in Figure 9 refer only to unconverted photons. The case of converted photons will be considered in Section 3.3.

$$\sin(\delta) = \sqrt{\frac{S_{major} - 0.304}{1.763}} \tag{7}$$

The uncertainty in the determination of $\sin(\delta)$ using Equation 7 is shown in Figure 11 as a function of $\sin(\delta)$. We use S_{major} in combination with T_{REC} to select off-pointing photons from the decay of a long-lived particle, where Figure 12 shows the distributions in the S_{MAJ} versus T_{REC} plane for Particle Gun and GMSB photons. Pointing photons are seen to populate regions at lower values of S_{major} and T_{REC}, whilst off-pointing photons populate areas at larger values. Hence, we settle on the following selection criteria in order to select off-pointing photons:

1. ECAL time requirement: $T_{REC} > 0.8$ ns
2. Major axis requirement: $S_{major} > 0.4$.

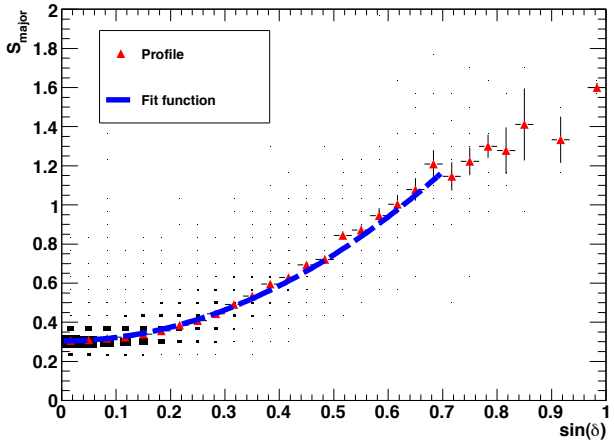

Figure 10: A scatter plot for S_{major} versus $\sin(\delta)$. The histogram profile is superimposed and fitted using a parabolic function.

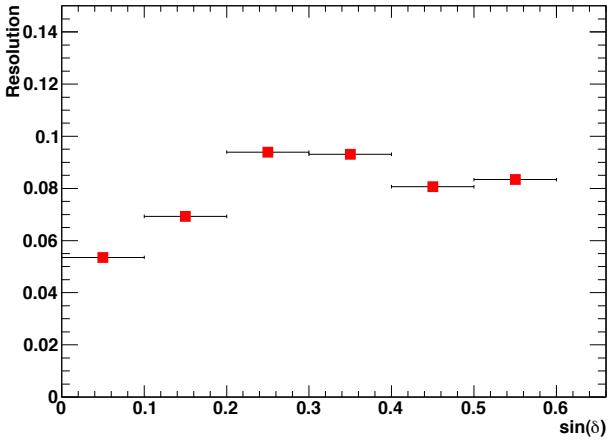

Figure 11: The uncertainty in the determination of the angle of incidence as a function of $\sin(\delta)$.

3.3 Identification of photon conversions

Photons conversions are a major background in this analysis as they are found to also produce ECAL clusters large values of S_{major} similar to off-pointing photons. This is due to the fact that the electron-positron pair is curved along ϕ direction due to the CMS magnetic field, and the energy of the incoming photon will be therefore shared

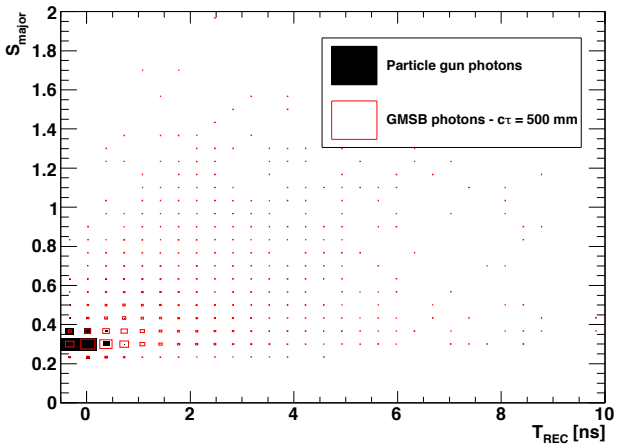

Figure 12: The S_{MAJ} versus T_{REC} distribution for Particle Gun and GMSB photons.

between a large number of crystals, resulting in a large S_{major} value. A common method for the identification of photon conversions uses $\sigma_{\phi\phi}$ (defined in Equation 3) as a discriminating variable, where Figure 13 shows the distribution of $\sigma_{\phi\phi}$ for unconverted and converted Particle Gun photons.

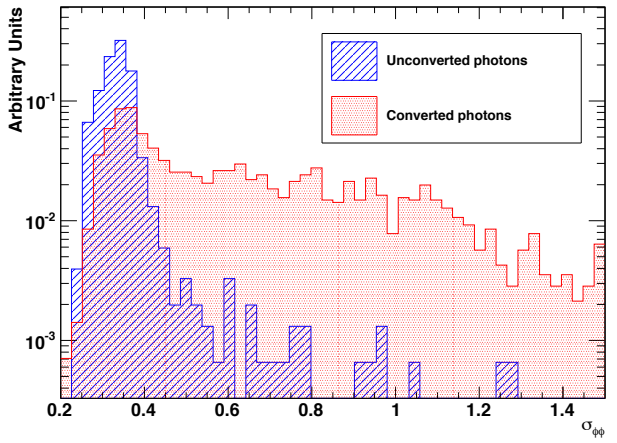

Figure 13: The $\sigma_{\phi\phi}$ distribution for unconverted and converted Particle Gun photons.

Despite the rejection power, $\sigma_{\phi\phi}$ cannot be used due to its strong relation to S_{major}. Therefore we use an alternative variable, not related to S_{major}, which is the angle α, defined as the angle between the ϕ direction and the major axis of the cluster. We calculate α from the covariance matrix using the following expression:

$$\tan\alpha = \frac{\sigma_{\eta\eta} - \sigma_{\phi\phi} + \sqrt{\left(\sigma_{\eta\eta} - \sigma_{\phi\phi}\right)^2 + 4\sigma_{\eta\phi}^2}}{2\sigma_{\eta\phi}} \tag{8}$$

The electron-positron pair produced is reconstructed as two bumps in the ECAL displaced along ϕ direction. This results in a very small angle between the ϕ direction and S_{major}. We expect the distribution of α to be a narrow peak at zero for converted photons, and to be distributed flatly for an unconverted photon. Figure 14 shows the distribution of α for clusters from (a) converted and (b) unconverted Particle Gun photons.

We see that α confirms our expectations for the case of converted photons, but the distribution for unconverted photons shows an unexpected peak at zero. This is due to the effect of the magnetic field on the electromagnetic shower inside the ECAL crystals, where the electrons produced during the development of the shower are curved along ϕ direction, causing an asymmetry between $\sigma_{\eta\eta}$ and $\sigma_{\phi\phi}$. The symmetry is restored when the magnetic field is switched off. Figure 15 shows the distributions in the $\sigma_{\phi\phi}$ versus $\sigma_{\eta\eta}$ plane for unconverted photons with the a) magnetic field switched on and b) magnetic field switched off.

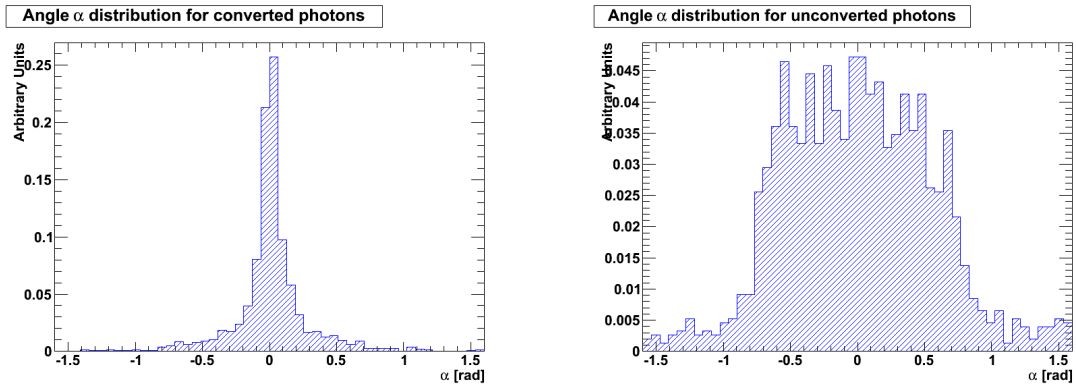

(a) (b)

Figure 14: The distribution of α for clusters from: a) converted; b) unconverted Particle Gun photons.

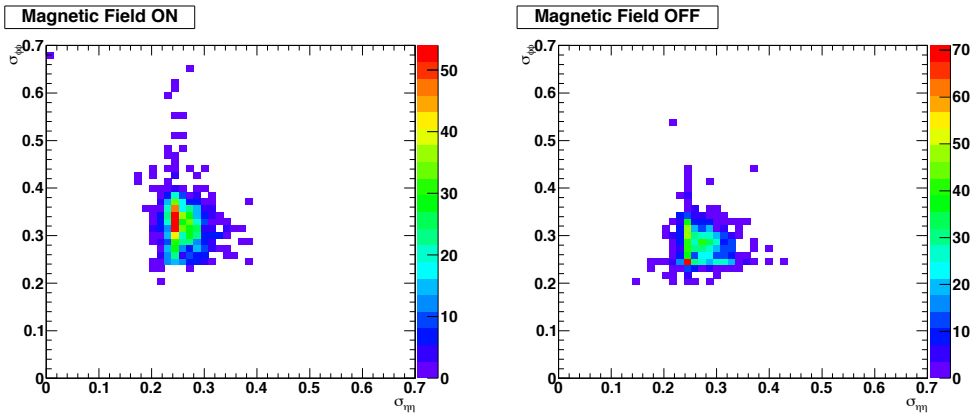

(a) (b)

Figure 15: The distribution for unconverted photons with the a) magnetic field switched on and b) magnetic field switched off in the $\sigma_{\phi\phi}$ versus $\sigma_{\eta\eta}$ plane.

We describe the effect of the magnetic field on the shape of unconverted photon clusters using the ratio between the mean value of $\sigma_{\eta\eta}$ and $\sigma_{\phi\phi}$:

$$K^2 = \frac{\langle \sigma_{\eta\eta} \rangle}{\langle \sigma_{\phi\phi} \rangle} = 0.838 \tag{9}$$

To restore the symmetry, we define the following modified covariance matrix:

$$COV^*_{\eta\phi} = \begin{pmatrix} \sigma_{\eta\eta} & K \cdot \sigma_{\eta\phi} \\ K \cdot \sigma_{\phi\eta} & K^2 \cdot \sigma_{\phi\phi} \end{pmatrix} \tag{10}$$

Replacing $\sigma_{\eta\phi}, \sigma_{\phi\phi}$ with $K \cdot \sigma_{\eta\phi}$, and $K^2 \cdot \sigma_{\phi\phi}$ in Equation 8 we obtain the angle α corrected for the effect of the magnetic field.

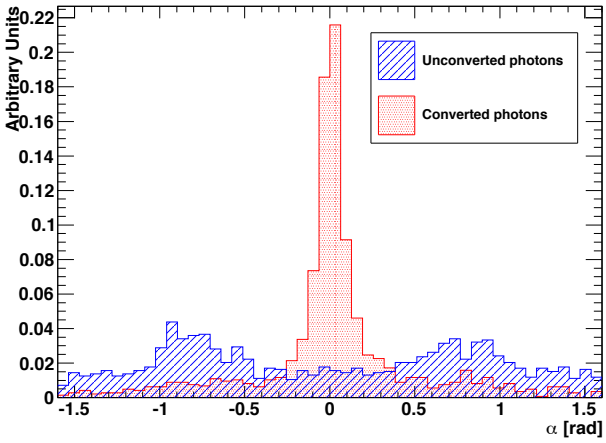

Figure 16: The distribution of α for unconverted and converted Particle Gun photons after the correction for the effect of the magnetic field.

We see in Figure 16 a comparison between α for unconverted and converted photons after the correction for the effect of magnetic field. We use the following selection cuts based on α to identify photon conversions:

- Unconverted photons: $|\alpha| > 0.3$;
- Converted photons: $|\alpha| < 0.3$.

4 Determination of the flight path of long-lived particles decaying into photons

We present an algorithm to extract the flight path of long-lived particles decaying into photons exploiting the excellent time determination, and the fine lateral granularity of the ECAL. The algorithm consists of two steps:

1. The reconstruction of the momentum of the off-pointing photon using the ECAL energy measurement, and the cluster shape variables (introduced in Section 3);
2. The determination of the coordinates of the long-lived particle decay vertex using the ECAL time measurement, and the flight direction of the photon obtained from the momentum reconstruction.

4.1 Reconstruction of the off-pointing photon momentum

The momentum of an off-pointing photon can be reconstructed using:

- The energy of the reconstructed cluster E_{CLU} (representing the absolute value of photon momentum);

- The angle δ between the axis of the ECAL crystal and the photon direction, which can be extracted from S_{major} according to Equation 7;
- The angle α between the major axis of the cluster and ϕ direction.

The photon momentum can be represented as projection on the ECAL surface $P^{\gamma}_{//}$ and the normal component P^{γ}_{T}, i.e. the projection on the axis of the ECAL crystal using the following equations:

$$\begin{aligned} P^{\gamma}_{//} &= E_{CLU} \cdot \sin(\delta) \\ P^{\gamma}_{T} &= E_{CLU} \cdot \cos(\delta) \end{aligned} \tag{11}$$

Moreover, the determination of the angle α between the major axis and ϕ direction can be used to calculate the kinematics of the photon. Figure 17 shows a scatter plot for the true value of α angle versus the reconstructed value (calculated using Equation 8), where only unconverted GMSB photons with $T_{REC} > 0.8$ ns and $S_{major} > 0.4$ are considered. Despite the strong correlation, we notice an unresolved issue whereby we see a distinctive 'X-shape' due to the fact that S_{major} only identifies the direction of the momentum projection on the ECAL surface, and not the verse.

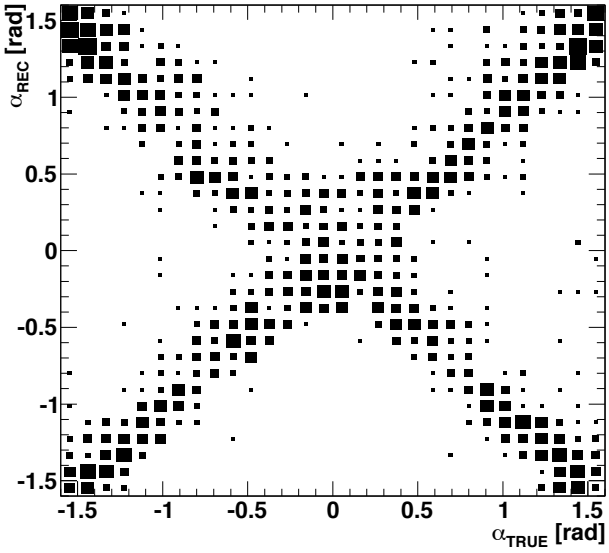

Figure 17: A scatter plot of α_{REC} versus α_{TRUE}.

Figure 18 shows α_{REC} versus α_{TRUE} where the ambiguity on the verse has been eliminated using Monte Carlo information on the photon momentum. Also, we can see the uncertainty on the determination of α angle in figure 19.

Although the ambiguity on the α determination produces a bias on the reconstruction of photon momentum, it will not impact the calculation of the flight path of long-lived particle. In fact, whilst a wrong determination of α will affect the determination of the photon momentum, the decay length of the long-lived particle can be calculated with a good accuracy using only the angle of incidence δ of the off-pointing photon.

4.2 Flight path calculation

Using the photon direction calculated in Section 4.1 we are able to extract the decay vertex, and subsequently the flight path for the long-lived particle. Focusing on GMSB events, we relate the reconstructed time to the sum of the neutralino and photon flight path as follows:

$$T_{REC} = \frac{D_{\chi^0_1}}{\beta_{\chi^0_1} \cdot c} + \frac{D_{\gamma}}{c} \tag{12}$$

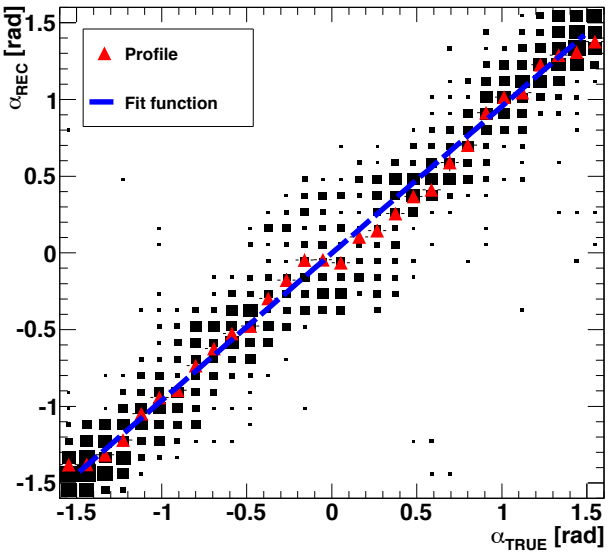

Figure 18: A scatter plot of α_{REC} versus α_{TRUE}. The correct verse for the major axis is chosen from Monte Carlo truth information. The histogram profile is superimposed and fitted using a linear function.

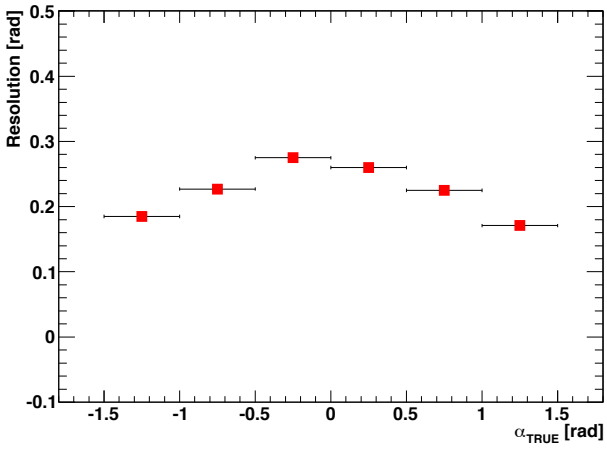

Figure 19: The uncertainty on the determination of α as a function of α_{TRUE}.

where D_{χ^0} and D_γ refer to the flight path of the neutralino and photon respectively, $v_{\chi_1^0}$ refers to the velocity of the neutralino, and c is the speed of the light. We see in Figure 20 a schematic view of the neutralino and photon flight paths.

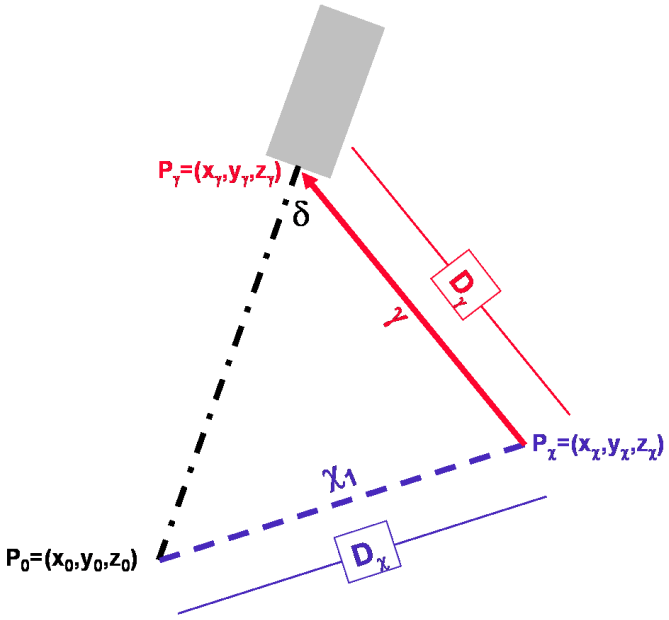

Figure 20: Schematic view of the neutralino and photon flight paths.

Following the notation introduced in Figure 20 the decay vertex of the neutralino can be expressed as:

$$\begin{aligned} x_{\chi_1^0} &= x_\gamma - \widehat{x}_\gamma \cdot t \\ y_{\chi_1^0} &= y_\gamma - \widehat{y}_\gamma \cdot t \\ z_{\chi_1^0} &= z_\gamma - \widehat{z}_\gamma \cdot t \end{aligned} \tag{13}$$

where $(x_\gamma, y_\gamma, z_\gamma)$ are the coordinates of the impact point of the photon on the ECAL surface, $(\widehat{x}_\gamma, \widehat{y}_\gamma, \widehat{z}_\gamma)$ is the versor representing the photon direction, and t is the parameter that coincides with the flight path of the photon. Additionally, the neutralino flight path can be written as a function of parameter t according to the following expression:

$$D_{\chi_1^0} = \overline{P_0 P_{\chi_1^0}} = \sqrt{((x_0 - x_\gamma + \widehat{x}_\gamma \cdot t)^2 + (y_0 - y_\gamma + \widehat{y}_\gamma \cdot t)^2 + (z_0 - z_\gamma + \widehat{z}_\gamma \cdot t)^2)} \tag{14}$$

Combining Equation 14 and Equation 12, and setting $D_\gamma = t$, we are able to express a second-order equation for t as follows:

$$T_{REC} = \frac{t}{c} + \frac{\sqrt{(x_0 - x_\gamma + \widehat{x}_\gamma \cdot t)^2 + (y_0 - y_\gamma + \widehat{y}_\gamma \cdot t)^2 + (z_0 - z_\gamma + \widehat{z}_\gamma \cdot t)^2}}{\beta_{\chi_1^0} \cdot c} \tag{15}$$

From 15 we see that the speed of the neutralino ($\beta_{\chi_1^0}$) is the only unknown variable. This is extracted using the correlation with the energy of the daughter photon from the χ_1^0. We see in Figure 21 that the reconstructed energy spectrum for the daughter photons [2)] (with $c\tau = 500$ mm). To reduce QCD backgrounds, only photons with $E_{CLU} > 50$ GeV are considered.

A relationship between the speed of neutralino and the photon energy can be established by fitting for the profile of $\beta_{\chi_1^0}$ versus E_{CLU} distribution, as shown in Figure 22.

The function used for the fit is expressed as:

[2)] The energy spectrum of the photon strongly depends on the mass of neutralino which is affected by the choice of the model parameters.

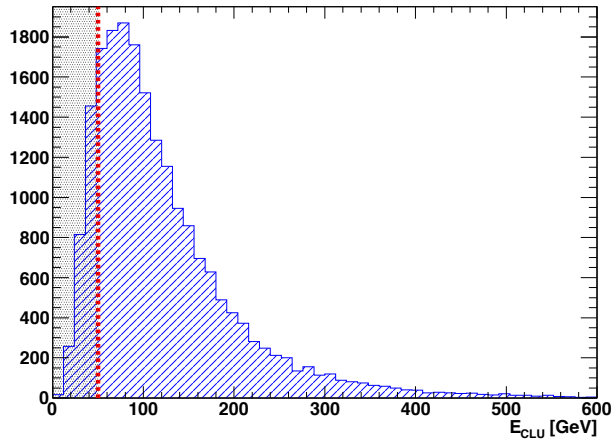

Figure 21: The reconstructed energy spectrum for photons from the χ_1^0 decay, using photons with $E_{CLU} > 50$ GeV.

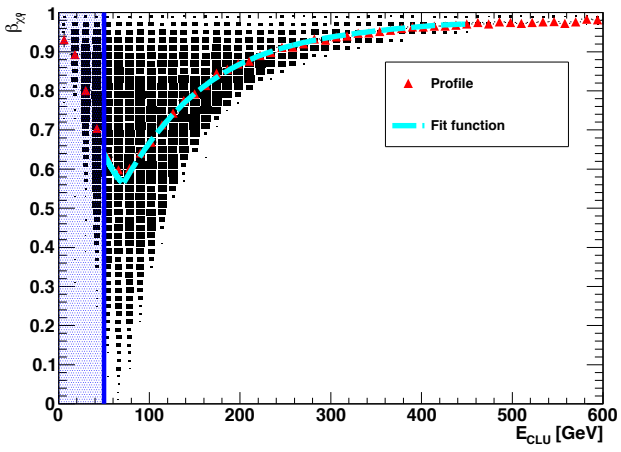

Figure 22: A scatter plot of $\beta_{\chi_1^0}$ versus E_{CLU}. The histogram profile is superimposed and fitted with a polynomial function.

$$\begin{aligned} \beta_{\chi_1^0} &= \tfrac{1}{c} \cdot (\textstyle\sum_{i=0}^{2} A_i \cdot E_{CLU}^i) \qquad 50 < E_{CLU} < 70GeV \\ \beta_{\chi_1^0} &= \tfrac{1}{c} \cdot (\textstyle\sum_{i=0}^{4} B_i \cdot E_{CLU}^i) \qquad E_{CLU} \geq 70GeV \end{aligned} \tag{16}$$

The fit parameters A_i and B_i are listed in Table 2 and Table 3 respectively.

A_0	A_1	A_2
$3.14 \cdot 10^{1}$	$-3.40 \cdot 10^{-1}$	$1.91 \cdot 10^{-3}$

Table 2: The fit parameters for $50 < E_{CLU} < 70$ GeV.

B_0	B_1	B_2	B_3	B_4
$5.02 \cdot 10^{0}$	$2.17 \cdot 10^{-1}$	$-7.98 \cdot 10^{-4}$	$1.39 \cdot 10^{-6}$	$-9.36 \cdot 10^{-10}$

Table 3: The fit parameters for $E_{CLU} > 70$ GeV.

The parameter t is extracted by taking the largest solution in Equation 15 and inputting this in Equation 14 to obtain the flight path $\beta\gamma ct_{REC}$ of the neutralino. Figure 23 shows the distribution of $\beta\gamma ct_{REC}$ for χ_1^0 with $c\tau = 500$ mm. The following selection for the reconstructed photon is used:

- $T_{REC} > 0.8$ ns and $S_{major} > 0.4$ (to select off-pointing photons);
- $|\alpha_{REC}| > 0.3$ (to select unconverted photons).

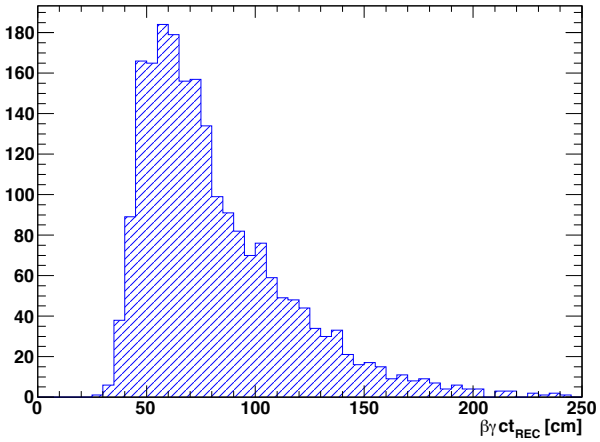

Figure 23: The distribution of the reconstructed flight path $\beta\gamma ct_{REC}$ using neutralinos with $c\tau = 500$ mm.

We see the performance of the algorithm described in this section from Figure 24, where the expected linear correlation between the reconstructed and true values of the neutralino flight path is shown. Figure 25 shows the uncertainty on the neutralino flight path calculation, where the distribution of $(\beta\gamma ct_{REC} - \beta\gamma ct_{TRUE})$ is fitted using a gaussian function and the resolution on the flight path calculation is $\sigma = 18.5$ cm. The distribution of $\beta\gamma ct_{REC}$ is shown in Figure 26, where we see that as the neutralino lifetime increases, $\beta\gamma ct_{REC}$ tends to similar values for the different chooses of the neutralino lifetime. Furthermore, we note that when the lifetime is comparable with the maximum length of the ECAL, an increasing number of neutralinos will decay outside the bounds of the ECAL producing an undetectable photon. Therefore, the distribution of the reconstructed flight path will have an upper limit dependent on the size of the ECAL.

Figure 27 shows the average value of the reconstructed flight path distribution ($\langle\beta\gamma ct_{REC}\rangle$) as a function of the neutralino lifetime. After a rapid increase of $\langle\beta\gamma ct_{REC}\rangle$ at small values of $c\tau$, the distribution is shown to plateau when the neutralino lifetime is comparable with the size of the ECAL. Once a relationship between $\langle\beta\gamma ct_{REC}\rangle$ and $c\tau$ has been established, the former can be used to determine the lifetime for the long-lived particle. However, this method is not productive at large neutralino lifetimes where we encounter a dramatic loss of sensitivity in the determination of $c\tau$.

We use the efficiency of the off-pointing photon selection to distinguish between different values of $c\tau$ when the the neutralino lifetime is too large to be reconstructed with a high accuracy (as shown in Figure 28). We can see

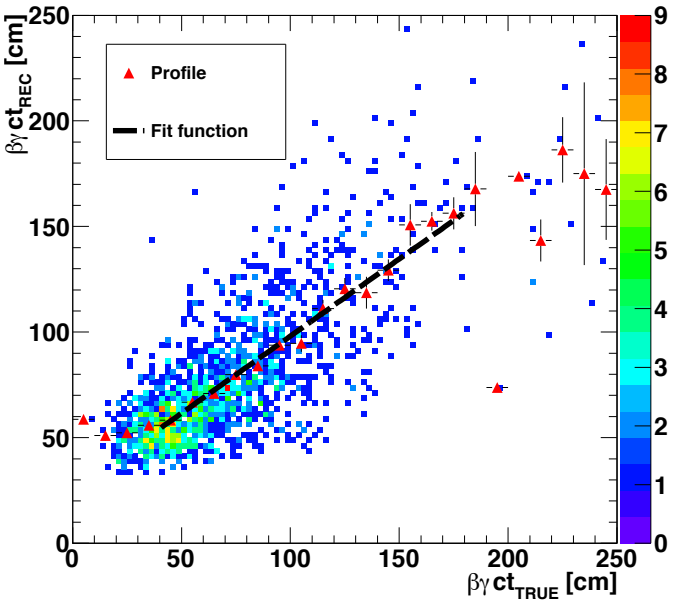

Figure 24: A scatter plot of $\beta\gamma ct_{REC}$ versus $\beta\gamma ct_{TRUE}$. The histogram profile is superimposed and fitted with a linear function.

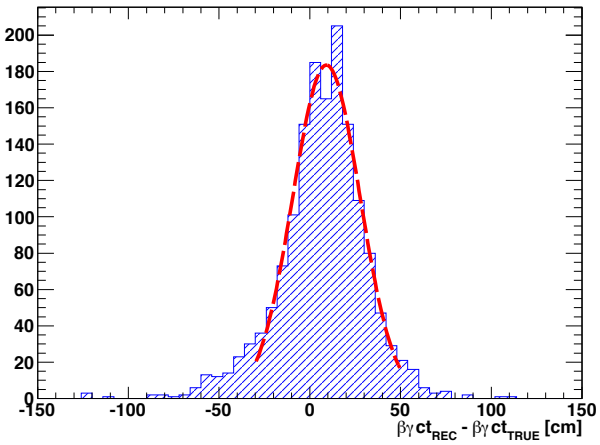

Figure 25: The uncertainty for the $\beta\gamma ct_{REC}$ calculation.

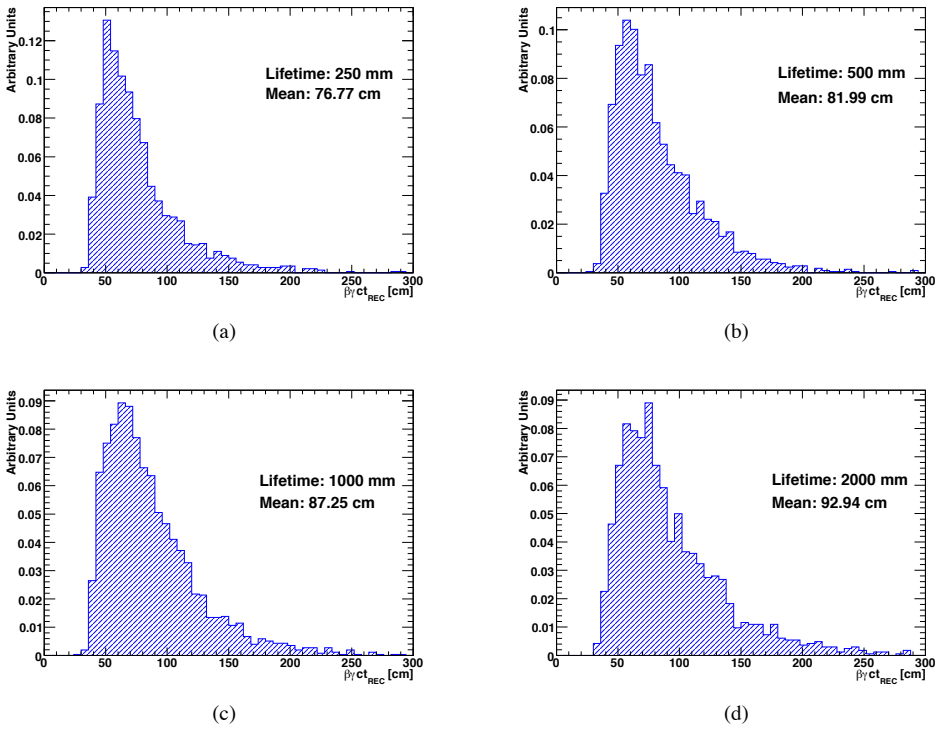

Figure 26: The $\beta\gamma ct_{REC}$ distribution for different values of the neutralino lifetime with: a) cτ = 250 mm; b) cτ = 500 mm; c) cτ = 1000 mm; d) cτ = 2000 mm.

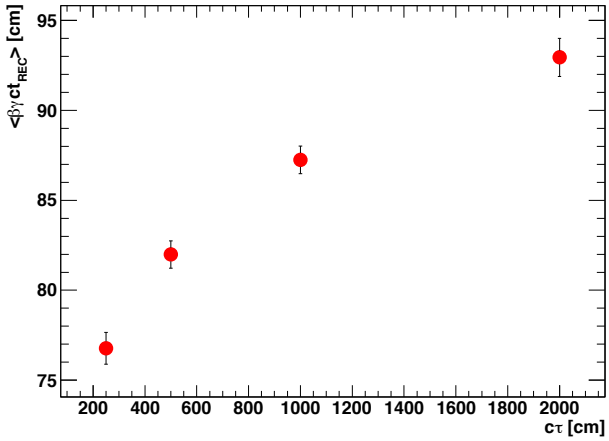

Figure 27: The $\langle\beta\gamma ct_{REC}\rangle$ distribution as a function of the neutralino lifetime.

that the efficiency strongly depends on the neutralino lifetime, where for small values of $c\tau$ the efficiency is very low due to the fact that most of the photons originate from the interaction point. We see an increase in the efficiency which reaches a maximum at around $c\tau = 1000$ mm, and then is seen to decrease (since most of the neutralinos will decay outside of the ECAL). Therefore, we use a combination of both $\beta\gamma c\tau_{REC}$ and the off-pointing selection efficiency should to calculate the neutralino lifetime.

In Figure 29 we see a plot of the efficiency for the off-pointing selection as a function of $c\tau$ for photons from neutralinos with a true flight path between than 40 and 100 cm and $\beta_{\chi_1^0} < 0.67$, where the true flight path and $\beta_{\chi_1^0}$ are obtained from Monte Carlo information. As expected, when we only consider true long-lived neutralinos, the efficiency of the off-pointing selection is not completely dependent on the value of $c\tau$.

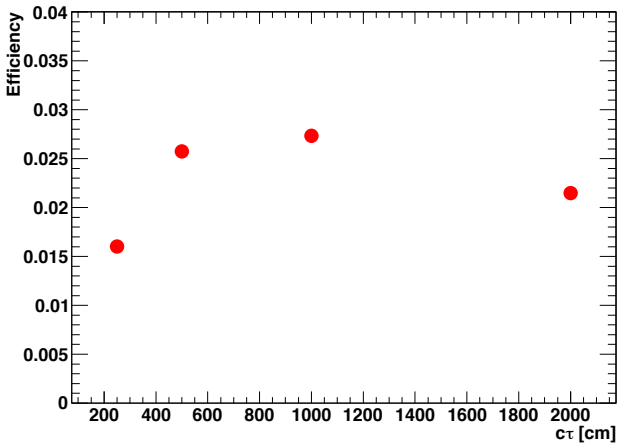

Figure 28: The efficiency of the off-pointing photon selection as a function of the neutralino lifetime.

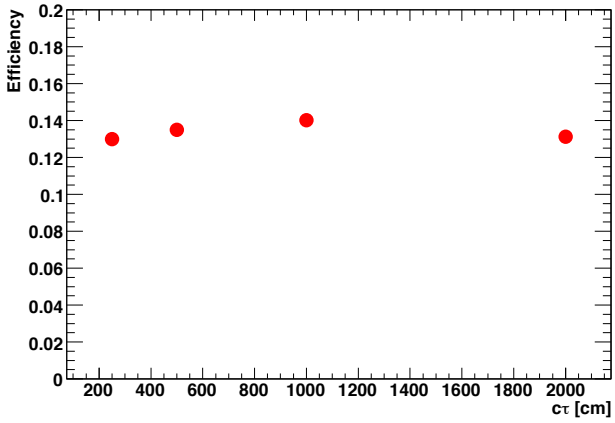

Figure 29: The efficiency of the off-pointing photon selection as a function of neutralino lifetime, where only neutralinos with a true flight path between than 40 and 100 cm and $\beta_{\chi_1^0} < 0.67$ are considered.

5 Conclusions

In summary, we present an algorithm which reconstructs the flight path of long-lived particles decaying into photons. The algorithm is model-independent, but our studies will focus on the Supersymmetric GMSB model where the long-lived particle is the neutralino which decays according to the following relation: $\chi_1^0 \rightarrow \tilde{G}\gamma$. We use the reconstructed ECAL time, and the cluster shape variable S_{major}, in order to select off-pointing photons. The angle between S_{major} and ϕ axis is then used to subtract background from photon conversions. The momentum for the off-pointing photons is determined using the reconstructed energy and the α and δ angles (calculated using cluster shape variables). which is used to with the ECAL time measurement in order to extract neutralino flight path.

References

[1] G. F. Giudice, R. Rattazzi, *Theories with gauge-mediated supersymmetry breaking*, Phys.Rept.322:419-499,1999, hep-ph/9801271.

[2] B. C. Allanach, *et al*., *The Snowmass Points and Slopes:benchmarks for SUSY searches*., Eur. Phys. J. C 25 (2002) 113, hep-ph/0202233.

[3] The CMS Collaboration, *Time reconstruction and performance of the CMS electromagnetic calorimeter*, CERN-CMS-PAPER CFT-09-009.

[4] The CMS Collaboration, *CMS Physics TDR, Volume 1*, CERN-LHCC 2006-001 (2006).

[5] D. Franci, S. Rahatlou, D. del Re, *Studies for photons and neutral pions identification in the ECAL barrel region*, CMS AN-2008/075.